The Astrophysical Journal, 759:96 (14pp), 2012 November 10 doi:10.1088/0004-637X/759/2/96


# THE ARECIBO H II REGION DISCOVERY SURVEY

T. M. Bania[1], L. D. Anderson[2], and Dana S. Balser[3]
[1] Institute for Astrophysical Research, Department of Astronomy, Boston University, 725 Commonwealth Ave., Boston, MA 02215, USA
[2] Department of Physics, West Virginia University, Morgantown, WV 26506, USA
[3] National Radio Astronomy Observatory, 520 Edgemont Road, Charlottesville, VA 22903-2475, USA
*Received 2012 August 17; accepted 2012 September 17; published 2012 October 23*

## ABSTRACT

We report the detection of radio recombination line (RRL) emission using the Arecibo Observatory at X band (9 GHz, 3 cm) from 37 previously unknown H II regions in the Galactic zone $66^\circ \geqslant \ell \geqslant 31^\circ$ and $|b| \leqslant 1^\circ$. This Arecibo H II Region Discovery Survey (Arecibo HRDS) is a continuation of the Green Bank Telescope (GBT) HRDS. The targets for the Arecibo HRDS have spatially coincident 24 $\mu$m and 20 cm emission of a similar angular morphology and extent. To take advantage of Arecibo's sensitivity and small beam size, sources in this sample are fainter, smaller in angle, or in more crowded fields compared to those of the GBT HRDS. These Arecibo nebulae are some of the faintest H II regions ever detected in RRL emission. Our detection rate is 58%, which is low compared to the 95% detection rate for GBT HRDS targets. We derive kinematic distances to 23 of the Arecibo HRDS detections. Four nebulae have negative local standard of rest velocities and are thus unambiguously in the outer Galaxy. The remaining sources are at the tangent-point distance or farther. We identify a large, diffuse H II region complex that has an associated H I and $^{13}$CO shell. The ~90 pc diameter of the G52L nebula in this complex may be the largest Galactic H II region known, and yet it has escaped previous detection.

*Key words:* Galaxy: structure – H II regions – ISM: bubbles – surveys – techniques: spectroscopic

*Online-only material:* color figures

## 1. INTRODUCTION

H II regions are the zones of plasma surrounding massive OB stars. Because such stars only live for a few Myr, H II regions are clear indicators of ongoing massive star formation. They are luminous objects at radio and infrared (IR) wavelengths and can be seen across the entire Galactic disk. Despite much effort, the census of Galactic H II regions is still incomplete. A complete census of Galactic H II regions is important if we are to use these nebulae to trace Galactic structure, to determine the Galactic high-mass star formation rate, and to characterize the Galactic H II region population as a whole.

Radio emission from H II regions is dominated by two emission mechanisms. H II region plasma emits radio continuum emission from thermal bremsstrahlung. Recombining electrons and nuclei in the plasma produce recombination line emission, which is observable from optical to radio wavelengths. Most surveys of H II regions over the past few decades were conducted using radio recombination line (RRL) emission, and the targets were identified from radio continuum maps (e.g., Reifenstein et al. 1970; Wilson et al. 1970; Caswell & Haynes 1987; Lockman 1989). Measuring an RRL gives a radial velocity that, when combined with a model of Galactic rotation, can be used to derive a kinematic distance (e.g., Wilson et al. 1970).

Dust in the H II region emits in the IR, especially the mid- to far-IR. This was demonstrated conclusively by Wood & Churchwell (1989), who measured radio continuum emission from ultra-compact H II regions spatially coincident with *IRAS* point sources. The combination of infrared and radio continuum emission strongly indicates that a source is emitting thermally, i.e., it is an H II region or a planetary nebula (PN) and not a supernova remnant or an active galactic nucleus (Haslam & Osborne 1987; Broadbent et al. 1989). More recent RRL surveys of H II regions used IR data to identify candidate targets (Araya et al. 2002; Watson et al. 2003; Sewilo et al. 2004; Anderson et al. 2011).

The H II Region Discovery Survey (HRDS) is an ongoing census program that aims to locate and measure the RRL emission from as many Galactic H II regions as possible. In the Green Bank Telescope (GBT) HRDS, we detected the RRL and continuum emission from 448 previously unknown Galactic H II regions at X band (9 GHz, 3 cm). This census doubles the number of known H II regions over the Galactic zone studied. Bania et al. (2010, hereafter Paper I) described the GBT HRDS survey. Anderson et al. (2011, hereafter Paper II) gave the GBT HRDS methodology and provided the HRDS source catalog. Anderson et al. (2012a, hereafter Paper III) derived kinematic distances to a large fraction of the GBT HRDS sample. Wenger et al. (2012) will give the properties of the helium and carbon RRLs detected in the GBT HRDS nebulae.

Here, we report the discovery of 37 previously unknown H II regions found by detecting RRL emission from targets using the Arecibo telescope at X band (9 GHz, 3 cm). With ~9 times the collecting area of the GBT, Arecibo has a higher sensitivity. Its beam is nearly three times smaller than that of the GBT. These factors make it possible for Arecibo to find H II regions that are fainter and smaller than GBT HRDS targets or are located in confused regions of the Galaxy.

## 2. TARGET SAMPLE

We define the Arecibo target sample in the same way as for the GBT HRDS, searching by eye for spatial coincidences between mid-infrared (MIR) and radio continuum sources. Sources with spatially coincident MIR and radio continuum emission are likely to be thermal emitters; the 95% detection rate of the GBT HRDS targets so defined confirms this. We use *Spitzer* MIPSGAL data (Carey et al. 2009) for the MIR and both 20 cm MAGPIS (Helfand et al. 2006) and 21 cm VLA Galactic Plane Survey data (VGPS; Stil et al. 2006) for the radio. MAGPIS has an angular resolution of ~5″, comparable to the MIPSGAL resolution of 6″, whereas the VGPS has an angular resolution

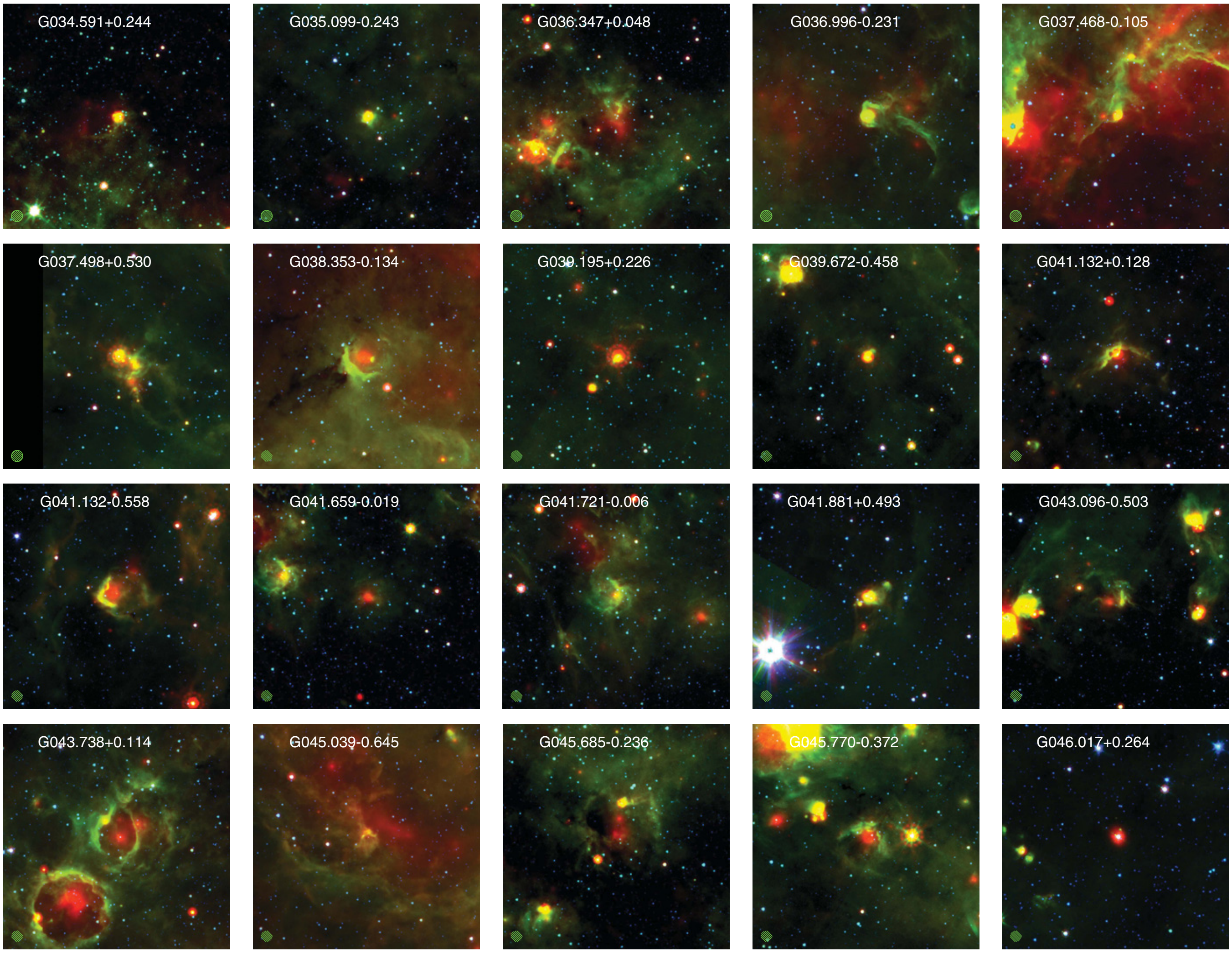


**Figure 1.** *Spitzer* infrared images of Arecibo HRDS nebulae. Image data are from MIPSGAL 24 $\mu$m (red), GLIMPSE 8.0 $\mu$m (green), and GLIMPSE 3.6 $\mu$m (blue). Each image is 12′ square; the 30″ Arecibo beam is shown in the lower left corner.

(A color version of this figure is available in the online journal.)

of 1′. Because the Arecibo beam at X band, ∼30″, is smaller than the resolution of the VGPS data, MAGPIS is helpful when attempting to identify candidates in crowded fields of IR and radio continuum emission. We show in Figure 1 three-color *Spitzer* MIR images for all of the new Arecibo H II region detections.

The Arecibo targets are fainter, smaller, or lie in more crowded fields compared with the GBT HRDS sources. The Arecibo gain at X band is ∼2.5 times that of the GBT; Arecibo can therefore, in principle, detect individual spectral lines from fainter sources than the GBT. The Arecibo beam at X band is ∼30″ compared to ∼82″ for the GBT. For sources compact with respect to the GBT beam, Arecibo will suffer less beam dilution and therefore should be more sensitive. In complicated fields, the GBT beam may include the emission from multiple H II regions along the line of sight. For these fields, the smaller Arecibo beam size can better measure the emission from a single H II region.

Our H II region candidate targets are located in the Galactic zone $66^\circ \geqslant \ell \geqslant 31^\circ$ and $|b| \leqslant 1^\circ$. These limits are set by the sky coverage of the Arecibo telescope and the MIPSGAL survey boundaries. The Arecibo declination limit of $\delta > -1^\circ\, 20'$ prevents observations of the Galactic plane below $\ell \sim 31^\circ$. The upper longitude limit and the latitude limit are set by the MIPSGAL survey boundaries. Finally, the MAGPIS survey extends only to $\ell < 48\overset{\circ}{.}5$, so we cannot use these 20 cm data for all candidates.

We observe the 63 targets that have the brightest expected X-band continuum fluxes. We compute these fluxes from aperture photometry of 21 cm VGPS data. These L-band fluxes are extrapolated to X band under the assumption that the emission at 21 cm is optically thin. In the GBT HRDS, we found that these extrapolated values disagree by as much as ∼±100% from the measured GBT X-band continuum intensities, possibly because the derived fluxes are poor or because the assumption that all sources are optically thin at 20 cm is invalid.

We detect RRL emission from 37 targets. Table 1 lists these H II regions and gives the source name, its Galactic and equatorial (J2000) coordinates, the velocity of detected CS 2 → 1 emission from Bronfman et al. (1996), and a characterization of the source morphology based on *Spitzer* GLIMPSE 8.0 $\mu$m images (Benjamin et al. 2003). The morphological classifications are the same as in Paper II. If the source is associated with a GLIMPSE bubble from Churchwell et al. (2006), then we give the bubble name in parentheses in the “morphology” column. Because CS emission is only detectable for dense molecular clouds, it is a good tracer of the early stages of star formation.

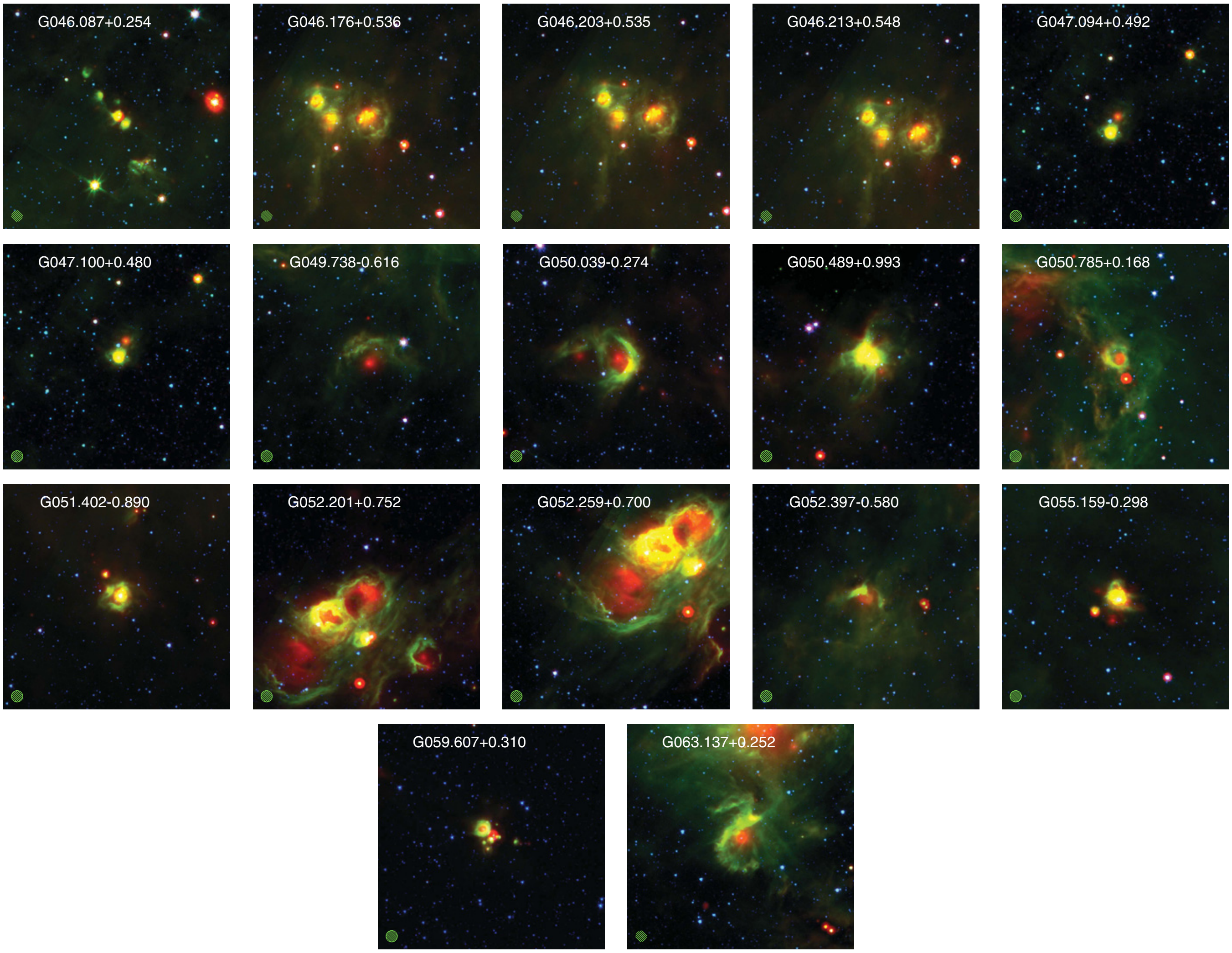


**Figure 1.** (Continued)

Paper II found good agreement between the CS and RRL velocities and also gave associations with 6.7 GHz methanol masers from Pestalozzi et al. (2005). No Arecibo HRDS sources have a methanol detection within 2′.

## 3. OBSERVATIONS AND DATA ANALYSIS

To make the Arecibo HRDS, we used the 305 m telescope during the period 2011 October to 2012 April. Each observing session consists of one sidereal pass of the first quadrant Galactic plane and lasts approximately five hours. At the beginning of each run, we make radio continuum cross-scans of the standard source B1843+09 to verify the observing setup, and to confirm that the measured gain is within the expected range, i.e., that the telescope is in focus. We also verify the spectral tunings by observing the bright H II region G045.455+0.059. As in Paper II, we use our custom IDL software package TMBIDL[4] to analyze these data.

The telescope gain depends on what part of the dish is illuminated. Because we are observing at the high-frequency limit of Arecibo, the changing rms of the surface that is being illuminated as a source is tracked can alter the gain by 20% or more. Furthermore, at low zenith angles, the telescope cannot track fast enough to remain pointed at the source, whereas at high zenith angles there is spillover. Both these situations also affect the telescope gain. The Arecibo gain at X band is in the range ∼4–6 K $\text{Jy}^{-1}$, depending on azimuth and zenith angle.[5] This gain variation motivates many of our choices for the observational setup and subsequent data analysis. First, we do not observe radio continuum from our sources as we did in the GBT HRDS. Such measurements would not be reliable without extensive calibration, and even then would likely be of low quality given the weather conditions we typically encounter. Second, we do not calibrate measured intensities with astronomical sources of known intensity, but instead rely solely on noise diodes to measure the system temperature. This again is difficult to do correctly with Arecibo, and would add little to the astrophysical importance of these data. The only reliably determined line parameter is the RRL local standard of rest (LSR) velocity. The RRL line intensity and line width should be used only with great caution.

We use the "Interim" correlator configured into sub-bands that are tuned to four consecutive RRL transitions, H 89 $\alpha$ to H 92 $\alpha$. We sample both circular polarizations for each tuning. We thus get eight independent spectra per observation: 4 RRLs × 2 orthogonal polarizations each. (For comparison, the GBT

4 See http://www.bu.edu/iar/tmbidl.

5 See http://www.naic.edu/∼astro/RXstatus/Xband/RX_xband.shtml

**Table 1**
Arecibo HRDS Source Catalog

| Name | $\ell$ (deg) | $b$ (deg) | R.A. (J2000) (hh:mm:ss.s) | Decl. (J2000) (dd:mm:ss) | CS[a] (km $s^{-1}$) | Morphology[b] |
|---|---|---|---|---|---|---|
| G034.591+0.244 | 34.591 | 0.244 | 18:53:35.9 | +01:35:17 | ... | C |
| G035.099–0.243 | 35.099 | −0.243 | 18:56:15.5 | +01:49:04 | ... | C |
| G036.347+0.048 | 36.347 | 0.048 | 18:57:30.0 | +03:03:39 | ... | I |
| G036.996–0.231 | 36.996 | −0.231 | 18:59:41.1 | +03:30:39 | ... | C |
| G037.468–0.105 | 37.468 | −0.105 | 19:00:05.9 | +03:59:19 | ... | C |
| G037.498+0.530 | 37.498 | 0.530 | 18:57:53.4 | +04:18:17 | ... | C |
| G038.353–0.134 | 38.353 | −0.134 | 19:01:49.7 | +04:45:43 | ND | B (N72) |
| G039.195+0.226 | 39.195 | 0.226 | 19:02:05.6 | +05:40:31 | 2.6 | C |
| G039.672–0.458 | 39.672 | −0.458 | 19:05:24.7 | +05:47:09 | ND | C |
| G041.132+0.128 | 41.132 | 0.128 | 19:06:01.0 | +07:21:05 | ... | PB |
| G041.132–0.558 | 41.132 | −0.558 | 19:08:28.4 | +07:02:11 | ... | B |
| G041.659–0.019 | 41.659 | −0.019 | 19:07:31.5 | +07:45:07 | ... | IB |
| G041.721–0.006 | 41.721 | −0.006 | 19:07:35.2 | +07:48:45 | ... | I |
| G041.881+0.493 | 41.881 | 0.493 | 19:06:05.7 | +08:11:04 | ... | C |
| G043.096–0.503 | 43.096 | −0.503 | 19:11:56.3 | +08:48:11 | ... | I |
| G043.738+0.114 | 43.738 | 0.114 | 19:10:55.5 | +09:39:27 | ... | B (N89) |
| G045.039–0.643 | 45.039 | −0.643 | 19:16:06.0 | +10:27:35 | ... | I |
| G045.685–0.236 | 45.685 | −0.236 | 19:15:51.7 | +11:13:12 | ... | IB |
| G045.770–0.372 | 45.770 | −0.372 | 19:16:30.7 | +11:13:55 | ... | B |
| G046.017+0.264 | 46.017 | 0.264 | 19:14:41.0 | +11:44:50 | ... | PS |
| G046.087+0.254 | 46.087 | 0.254 | 19:14:51.2 | +11:48:15 | ... | C |
| G046.176+0.536 | 46.176 | 0.536 | 19:13:60.0 | +12:00:50 | ... | B |
| G046.203+0.535 | 46.203 | 0.535 | 19:14:03.5 | +12:02:13 | ... | IB |
| G046.213+0.548 | 46.213 | 0.548 | 19:14:01.7 | +12:03:10 | ... | IB |
| G047.094+0.492 | 47.094 | 0.492 | 19:15:54.6 | +12:48:24 | ND | B |
| G047.100+0.480 | 47.100 | 0.480 | 19:15:57.8 | +12:48:21 | ND | C |
| G049.738–0.616 | 49.738 | −0.616 | 19:25:03.0 | +14:37:11 | ... | B |
| G050.039–0.274 | 50.039 | −0.274 | 19:24:23.5 | +15:02:49 | ... | B (N104) |
| G050.489+0.993 | 50.489 | 0.993 | 19:20:38.2 | +16:02:29 | ... | BB |
| G050.785+0.168 | 50.785 | 0.168 | 19:24:14.6 | +15:54:48 | ... | B (N106) |
| G051.402–0.890 | 51.402 | −0.890 | 19:29:20.1 | +15:57:07 | ... | B |
| G052.201+0.752 | 52.201 | 0.752 | 19:24:53.7 | +17:26:15 | ... | B |
| G052.259+0.700 | 52.259 | 0.700 | 19:25:12.1 | +17:27:48 | ... | B |
| G052.397–0.580 | 52.397 | −0.580 | 19:30:11.5 | +16:58:27 | ... | IB |
| G055.159–0.298 | 55.159 | −0.298 | 19:34:45.7 | +19:31:46 | 41.1 | C |
| G059.603+0.911 | 59.603 | 0.911 | 19:39:34.8 | +23:59:47 | 36.9 | B |
| G063.137+0.252 | 63.137 | 0.252 | 19:49:56.0 | +26:43:39 | ... | IB |

**Notes.**
[a] From Bronfman et al. (1996); "ND" means observed CS positions that lack emission.
[b] Morphological source structure classification based on *Spitzer* GLIMPSE 8 $\mu$m images: B: bubble: 8 $\mu$m emission surrounding 24 $\mu$m and radio continuum emission; BB: bipolar bubble: two bubbles connected by a region of strong IR and radio continuum emission; PB: partial bubble: similar to "B" but not complete; IB: irregular bubble: similar to "B" but with less well-defined structure; C: compact: resolved 8 $\mu$m emission with no hole in the center; PS: point source: unresolved 8 $\mu$m emission; I: irregular: complex morphology not easily classified. We list in parenthesis the bubble identification name for sources in the Churchwell et al. (2006) IR bubble catalog.

HRDS observed seven RRL transitions simultaneously, H 87 $\alpha$ to H 93 $\alpha$.) Each sub-band has a 25 MHz total bandwidth and its 1024 channels are nine-level sampled. The velocity resolution of all sub-bands is $\sim$0.8 km $s^{-1}$ per channel. Because the source velocities are unknown, we tune all sub-bands to a 0 km $s^{-1}$ LSR center velocity, which gives us a velocity coverage of $\sim\pm400$ km $s^{-1}$. Over the survey zone, this velocity range is more than sufficient to detect emission from all Galactic H II regions bound to the Galaxy.

We observe in total-power, position switching mode with on- and off-source integrations of five minutes each, hereafter a "pair." The off-source position is chosen so that we track the same azimuth and zenith angle path as the on-source scan does. We set the total integration time individually for each source based on the strength (or absence) of RRL emission. Total source integration times range from 1200 to 5400 s, with an average of 1800 s. Each individual pair is calibrated by firing the noise diodes.

About two hours of data were unusable due to rain storms and it was cloudy or lightly raining for most observing runs. X band is the highest radio frequency band observable with Arecibo and focusing the telescope is especially important compared to the lower frequencies. The Arecibo telescope is focused by using "tie down" cables running from each vertex of the triangular receiver platform to the ground. For 20% of our observing runs, the tie down system was not operational and the focus was not optimal. Finally, two of our observing runs are plagued by baseline ripples. These ripples appear in all sub-bands, although they are only readily apparent in the right circularly polarized data. The ripples have amplitudes of $\sim$5 mK and are present for

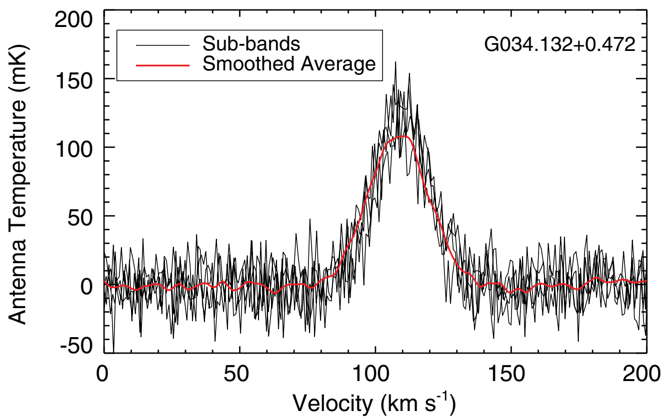


**Figure 2.** G034.132+0.472 H ii region spectra. Shown in black are spectra for the four different tunings (sub-bands). Each is the average of both circular polarizations. The red line ⟨ H n α ⟩ spectrum is the average of these data smoothed to 4.2 $km\,s^{-1}$ resolution.

(A color version of this figure is available in the online journal.)

most (but not all) of the two aforementioned days. We expunge almost all of these data in subsequent analyses. We do not know the source of these ripples.

To first order, RRLs at X band all have the same intensity, line width, and velocity; they can therefore be combined to create more sensitive ⟨ H n α ⟩ spectra. Because of their tunings, each sub-band has a slightly different spectral resolution, which complicates the process of averaging the individual spectral lines. In Paper II, we followed Balser (2006) and interpolated data from all sub-bands to that of the sub-band with the lowest velocity resolution. Here, for the H 89 α sub-band, the spectral resolution is 0.798 $km\,s^{-1}$, whereas it is 0.881 $km\,s^{-1}$ for the H 92 α sub-band. For an average RRL line width of 25 $km\,s^{-1}$ (see Paper II), the difference between the H 89 α sub-band and the H 92 α sub-band for this line width is three channels, or ∼2.5 $km\,s^{-1}$. Because we smooth the ⟨ H n α ⟩ spectra to a 4.2 $km\,s^{-1}$ resolution (see below), the difference in velocity resolution between the four sub-bands is unimportant and we do not perform any interpolation. All four sub-bands are Doppler tracked and have the same center velocity. The line velocities are therefore unaffected by the different spectral resolutions. We calculate average spectra in the standard way with a weighting factor of $t_{\rm intg}/T_{\rm sys}^2$, where $t_{\rm intg}$ is the integration time and $T_{\rm sys}$ is the total system temperature. Figure 2 shows an example of our analysis for the H ii region G034.132+0.472. The black lines show spectra for the four tunings (sub-bands). Each is the average of both circular polarizations. The average ⟨ H n α ⟩ spectrum is drawn in red.

We smooth the ⟨ H n α ⟩ spectra using a normalized Gaussian function of FWHM five channels to give a spectrum with a velocity resolution of 4.2 $km\,s^{-1}$. RRLs average ∼25 $km\,s^{-1}$ FWHM (see Paper II) so this guarantees that for most sources we have at least five spectral resolution elements across the line. We remove a polynomial baseline from the combined, smoothed spectrum. We determine the polynomial baseline order individually for each source, but it is generally third order or less. We then fit Gaussian functions to detected lines individually for each source. This gives us the LSR velocity, line intensity, and line width for each emission component. There are no other strong atomic, molecular, or unidentified lines known in these frequency bands and therefore the brightest detected lines are hydrogen RRLs. Finally, the Arecibo beam size changes with frequency so we might be sampling slightly different volumes of space with each tuning. Between the four sub-bands, the Arecibo beam is 10% different. As in the GBT HRDS, we do not attempt to correct for this effect.

## 4. THE ARECIBO H ii REGION DISCOVERY SURVEY CATALOG

We detect RRL emission from 37 sources out of 64 observed targets, a 58% success rate. We show these ⟨ H n α ⟩ spectra in Figure 3. Two sources have two RRL velocity components so the Arecibo HRDS contains 39 discrete RRLs altogether. The average rms noise for the survey ⟨ H n α ⟩ spectra is 2.0 mK. Given the Arecibo X-band gain of ∼4 K Jy, this corresponds to 0.5 mJy. For comparison, the GBT HRDS has a 95% detection rate and an average rms of 1.0 mJy.

Table 2 gives the Arecibo HRDS catalog hydrogen RRL line parameters, which come from Gaussian fits to the ⟨ H n α ⟩ spectra. It lists the source name, Galactic coordinates, line intensity, FWHM line width, LSR velocity, and the rms noise in the spectrum. Errors in line parameters are the $\pm 1\sigma$ uncertainties from the Gaussian fits. As we describe in Section 3, only the LSR velocity is reliably determined. The errors given in Table 2 for the line intensity and FWHM line width underestimate the true errors in these parameters. For the two sources with multiple RRL velocity components, we append an "a" or a "b" to the source names, in order of decreasing LSR velocity. We list the sources for which we did not detect RRL emission in Table 3, which gives the source name, Galactic position, rms noise, and GLIMPSE 8 $\mu$m morphology.

We re-observed a sample of GBT HRDS nebulae in order to verify the telescope configuration, to evaluate the data processing accuracy, and to cross-calibrate the two surveys. Table 4 lists hydrogen RRL parameters for four nebulae common to both surveys. Because of the different beam sizes, observations with the GBT and Arecibo potentially sample different volumes for a given source so we do not necessarily expect the line parameters to agree exactly. We are also comparing antenna temperature and not flux density, so we would not expect the line intensities to agree in these units. Moreover, given the gain variations of the Arecibo telescope, comparing the line intensities provides no useful insights. The agreement is, however, quite good for the RRL velocity and line width, although it is best for the brightest nebula, G034.133+0.471. For these sources, the mean absolute difference in velocity is 0.6 $km\,s^{-1}$ and the mean absolute difference in FWHM line width is 2.7 $km\,s^{-1}$. The line width is larger for all the Arecibo observations, which is due to how the four RRLs are averaged.

## 5. DISTANCES

We derive kinematic distances to the Arecibo HRDS nebulae as in Paper III. Kinematic distances are computed from models of Galactic rotation that take as inputs the source Galactic longitude and LSR velocity. Although some models also use the Galactic latitude to account for vertical deviations in Galactic rotational velocities, (e.g., Levine et al. 2008), we do not use them. As was also the case for the GBT HRDS, kinematic distances are the only method that can be used to derive distances to the majority of Arecibo HRDS sources. We compute all kinematic distances here using the Brand (1986, hereafter B86) rotation curve.

For sources in the inner Galaxy, there are two possible kinematic distances for each measured velocity, a "near" and a "far" distance. The "near" and the "far" distances for a given

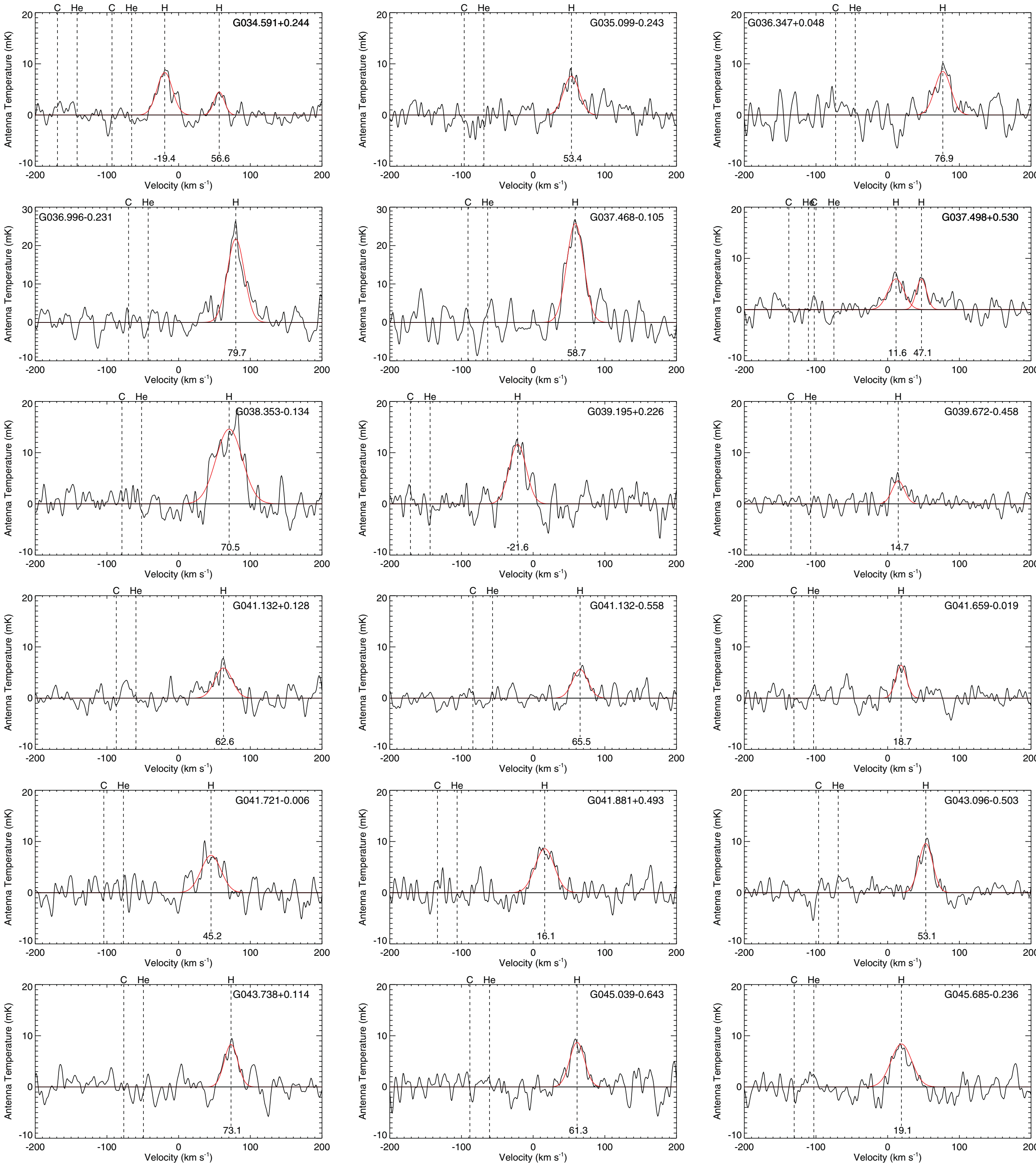


**Figure 3.** Arecibo HRDS composite ⟨ H n $\alpha$ ⟩ RRL discovery spectra. Shown is the average of the H 89 $\alpha$ through H 92 $\alpha$ RRLs, smoothed to 4.2 km s$^{-1}$ resolution. A Gaussian fit to each hydrogen RRL component is superimposed in red. A vertical dashed line flags the nebula's hydrogen RRL LSR velocity, which is listed at the bottom of the flag. The expected locations of the helium and carbon RRLs are also flagged.

(A color version of this figure is available in the online journal.)

line of sight are spaced equally about the tangent-point distance, which is the location of maximum radial velocity. This problem is known as the kinematic distance ambiguity (KDA). Without additional information, it is unknown which distance is correct for a given nebula. The outer Galaxy has no KDA, however, so our first Galactic quadrant Arecibo HRDS sources with negative RRL velocities are unambiguously in the outer Galaxy. We can derive kinematic distances for them directly from their measured velocities.

The H I Emission/Absorption (H I E/A) method has proved to be very effective at resolving the KDA for H II regions (see Kuchar & Bania 1994; Kolpak et al. 2003;

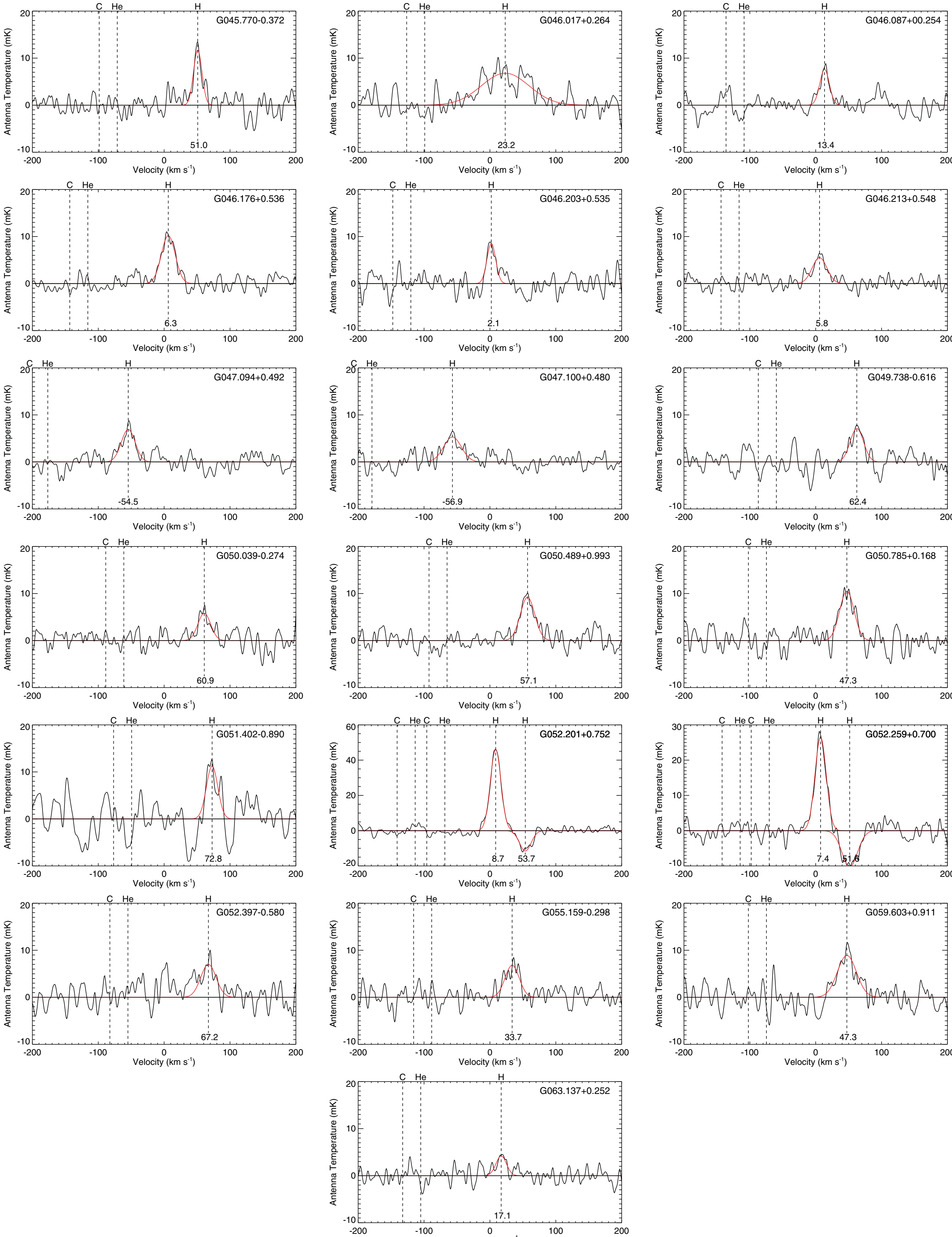


**Figure 3.** (Continued)

**Table 2**
Arecibo HRDS Hydrogen Recombination Line Parameters

| Name | $\ell$ (deg) | $b$ (deg) | $T_L$ (mK) | $\sigma T_L$ (mK) | $\Delta V$ (km s$^{-1}$) | $\sigma \Delta V$ (km s$^{-1}$) | $V_{\rm LSR}$ (km s$^{-1}$) | $\sigma V_{\rm LSR}$ (km s$^{-1}$) | rms (mK) |
|---|---|---|---|---|---|---|---|---|---|
| G034.591+0.244a | 34.591 | 0.244 | 4.5 | 0.4 | 17.0 | 1.6 | 56.6 | 0.7 | 1.2 |
| G034.591+0.244b | 34.591 | 0.244 | 8.3 | 0.3 | 25.4 | 1.1 | −19.4 | 0.5 | 1.2 |
| G035.099–0.243 | 35.099 | −0.243 | 7.6 | 0.3 | 25.8 | 1.2 | 53.4 | 0.5 | 1.8 |
| G036.347+0.048 | 36.347 | 0.048 | 8.5 | 0.4 | 26.5 | 1.4 | 76.9 | 0.6 | 2.1 |
| G036.996–0.231 | 36.996 | −0.231 | 21.7 | 0.6 | 28.0 | 0.9 | 79.7 | 0.4 | 2.1 |
| G037.468–0.105 | 37.468 | −0.105 | 25.7 | 0.5 | 28.0 | 0.6 | 58.7 | 0.3 | 3.3 |
| G037.498+0.530a | 37.498 | 0.530 | 6.0 | 0.3 | 16.6 | 0.9 | 47.1 | 0.4 | 1.5 |
| G037.498+0.530b | 37.498 | 0.530 | 6.0 | 0.2 | 26.4 | 1.2 | 11.6 | 0.5 | 1.5 |
| G038.353–0.134 | 38.353 | −0.134 | 14.6 | 0.6 | 43.2 | 2.0 | 70.5 | 0.8 | 1.9 |
| G039.195+0.226 | 39.195 | 0.226 | 11.6 | 0.5 | 27.9 | 1.3 | −21.6 | 0.6 | 2.1 |
| G039.672–0.458 | 39.672 | −0.458 | 4.5 | 0.4 | 20.2 | 2.4 | 14.7 | 1.0 | 1.4 |
| G041.132+0.128 | 41.132 | 0.128 | 5.9 | 0.3 | 28.4 | 1.7 | 62.6 | 0.7 | 1.4 |
| G041.132–0.558 | 41.132 | −0.558 | 5.6 | 0.2 | 25.3 | 0.9 | 65.5 | 0.4 | 1.3 |
| G041.659–0.019 | 41.659 | −0.019 | 6.4 | 0.3 | 17.9 | 0.9 | 18.7 | 0.4 | 1.4 |
| G041.721–0.006 | 41.721 | −0.006 | 7.3 | 0.4 | 32.6 | 2.3 | 45.2 | 0.9 | 1.8 |
| G041.881+0.493 | 41.881 | 0.493 | 8.6 | 0.2 | 31.6 | 1.1 | 16.1 | 0.4 | 1.7 |
| G043.096–0.503 | 43.096 | −0.503 | 9.6 | 0.3 | 23.0 | 1.0 | 53.1 | 0.4 | 1.5 |
| G043.738+0.114 | 43.738 | 0.114 | 8.3 | 0.3 | 22.4 | 0.9 | 73.1 | 0.4 | 1.7 |
| G045.039–0.643 | 45.039 | −0.643 | 8.7 | 0.3 | 24.6 | 0.9 | 61.3 | 0.4 | 1.8 |
| G045.685–0.236 | 45.685 | −0.236 | 8.4 | 0.3 | 34.0 | 1.3 | 19.1 | 0.5 | 1.6 |
| G045.770–0.372 | 45.770 | −0.372 | 11.7 | 0.6 | 15.1 | 0.9 | 51.0 | 0.4 | 1.9 |
| G046.017+0.264 | 46.017 | 0.264 | 6.8 | 0.3 | 85.2 | 4.4 | 23.2 | 1.7 | 2.2 |
| G046.087+0.254 | 46.087 | 0.254 | 7.6 | 0.3 | 17.0 | 0.9 | 13.4 | 0.4 | 1.8 |
| G046.176+0.536 | 46.176 | 0.536 | 10.2 | 0.2 | 24.8 | 0.6 | 6.3 | 0.2 | 1.2 |
| G046.203+0.535 | 46.203 | 0.535 | 8.5 | 0.6 | 15.7 | 1.2 | 2.1 | 0.5 | 1.9 |
| G046.213+0.548 | 46.213 | 0.548 | 5.5 | 0.2 | 26.3 | 1.3 | 5.8 | 0.6 | 1.4 |
| G047.094+0.492 | 47.094 | 0.492 | 6.9 | 0.3 | 24.8 | 1.3 | −54.5 | 0.5 | 1.4 |
| G047.100+0.480 | 47.100 | 0.480 | 5.3 | 0.2 | 31.6 | 1.7 | −56.9 | 0.7 | 1.4 |
| G049.738–0.616 | 49.738 | −0.616 | 7.1 | 0.3 | 23.9 | 1.2 | 62.4 | 0.5 | 2.1 |
| G050.039–0.274 | 50.039 | −0.274 | 5.8 | 0.4 | 22.7 | 1.7 | 60.9 | 0.7 | 1.9 |
| G050.489+0.993 | 50.489 | 0.993 | 9.2 | 0.3 | 25.9 | 1.1 | 57.1 | 0.5 | 1.5 |
| G050.785+0.168 | 50.785 | 0.168 | 10.5 | 0.4 | 25.8 | 1.2 | 47.3 | 0.5 | 2.1 |
| G051.402–0.890 | 51.402 | −0.890 | 11.2 | 0.8 | 20.5 | 0.2 | 72.8 | 0.7 | 3.5 |
| G052.201+0.752 | 52.201 | 0.752 | 46.1 | 0.5 | 19.0 | 0.2 | 8.7 | 0.1 | 1.6 |
| G052.259+0.700 | 52.259 | 0.700 | 26.5 | 0.4 | 20.0 | 0.4 | 7.4 | 0.1 | 1.9 |
| G052.397–0.580 | 52.397 | −0.580 | 7.0 | 0.4 | 27.4 | 2.3 | 67.2 | 0.8 | 1.9 |
| G055.159–0.298 | 55.159 | −0.298 | 6.8 | 0.4 | 25.3 | 1.7 | 33.7 | 0.7 | 1.7 |
| G059.603+0.911 | 59.603 | 0.911 | 8.9 | 0.3 | 34.1 | 1.6 | 47.3 | 0.6 | 2.1 |
| G063.137+0.252 | 63.137 | 0.252 | 4.2 | 0.4 | 18.7 | 1.8 | 17.1 | 0.8 | 1.3 |

Anderson & Bania 2009). In Paper III, we determined distances to 158 GBT HRDS sources by the H I E/A method using H I data from the VGPS. The H I E/A method relies on the detection of H I absorption of the broadband thermal radio continuum emission from an H II region. H I is ubiquitously distributed in the Galaxy and so it emits at all velocities permitted by Galactic rotation. If H I absorption is found between the nebular RRL velocity and the tangent-point velocity, then this favors the far distance. The absence of any H I absorption beyond the nebular RRL velocity favors the near distance. For the H I E/A method to be successful, however, the H II region must be bright enough to allow for detectable absorption.

We are able to derive kinematic distances for 23 Arecibo H II regions, which is 62% of the HRDS sample. Only three, however, have bright enough continuum emission to make an H I E/A analysis. For the other sources, we can establish kinematic distances to them because they are near the tangent-point distance, in the outer Galaxy (or very near to the solar orbit), or associated with large star-forming complexes with previously known distances.

Two of the H I E/A sources, G052.201+0.752 and G052.259+0.700, are in the G52 complex (see Section 6.4). Both of their RRL velocities are near 10 km s$^{-1}$ and H I absorption is detected up to 60 km s$^{-1}$, thus favoring the far distance. The third source, G041.881+0.493, has an RRL velocity of 23.2 km s$^{-1}$ and H I absorption is detected up to 68 km s$^{-1}$. This again favors the far distance. Paper III assigned "quality factors" (QFs) to assess the reliability of an H I E/A KDA determination. Using these same qualitative criteria, the H I E/A KDA resolution for these three nebulae would all be of the highest quality, QF "A."

As we did in Anderson & Bania (2009) and Paper III, we assign the tangent-point distance to the 12 Arecibo HRDS sources whose velocities are within 10 km s$^{-1}$ of the tangent-point velocity. For sources near the tangent point, our ability to discriminate between the near and far kinematic distances using the H I E/A method is limited. Furthermore, as the LSR velocity approaches the tangent-point velocity, the difference between the near and far distances becomes small so resolving the KDA is less important.

The four Arecibo HRDS sources with negative RRL velocities are unambiguously in the outer Galaxy. One of these, G034.591+0.244, has two RRL velocity components: 56.6 km s$^{-1}$ and −19.4 km s$^{-1}$. We believe that the latter is the actual velocity of this nebula and that the 56.6 km s$^{-1}$

**Table 3**
Targets Not Detected in RRL Emission

| Name | $l$ (deg) | $b$ (deg) | rms (mK) | Morphology[a] |
|---|---|---|---|---|
| G031.727+0.699 | 31.727 | 0.699 | 2.0 | B |
| G034.047+0.139 | 34.047 | 0.139 | 2.3 | PB |
| G037.319+0.162 | 37.319 | 0.162 | 2.2 | C |
| G038.906–0.437 | 38.906 | −0.437 | 2.4 | B (N74) |
| G038.977–0.269 | 38.977 | −0.269 | 2.1 | I |
| G039.271+0.347 | 39.271 | 0.347 | 1.9 | C |
| G039.506–0.280 | 39.506 | −0.280 | 2.2 | C |
| G040.017–0.119 | 40.017 | −0.119 | 2.0 | C |
| G040.422–0.039 | 40.422 | −0.039 | 2.6 | B (N77) |
| G041.229+0.170 | 41.229 | 0.170 | 2.2 | B |
| G044.244–0.129 | 44.244 | −0.129 | 1.9 | B |
| G044.353+0.443 | 44.353 | 0.443 | 2.2 | I |
| G044.775–0.548 | 44.775 | −0.548 | 3.7 | B (N93) |
| G046.060+0.220 | 46.060 | 0.220 | 2.8 | I |
| G047.183+0.317 | 47.183 | 0.317 | 2.0 | I |
| G050.900+1.056 | 50.900 | 1.056 | 1.8 | I |
| G056.252–0.160 | 56.252 | −0.160 | 2.7 | C |
| G056.255–0.099 | 56.255 | −0.099 | 2.8 | I |
| G057.469+0.304 | 57.469 | 0.304 | 1.9 | IB |
| G058.121+0.911 | 58.121 | 0.911 | 1.9 | C |
| G058.606+0.620 | 58.606 | 0.620 | 1.5 | PB |
| G059.607+0.310 | 59.607 | 0.310 | 2.8 | IB (N126) |
| G059.885+0.759 | 59.885 | 0.759 | 2.2 | B |
| G060.653–0.016 | 60.653 | −0.016 | 1.9 | PB (N127) |
| G062.370–0.540 | 62.370 | −0.540 | 2.0 | PB (N130) |
| G062.723+0.619 | 62.723 | 0.619 | 1.7 | IB |

**Note.** [a] Source structure classification as in Table 1.

component comes from diffuse gas along the line of sight. This is because there is no evidence for any spatially extended, diffuse gas in the outer disk for this part of the Milky Way, whereas the GBT HRDS catalog shows many examples of extended, diffuse gas in the first quadrant inner Galaxy. This negative velocity for G034.591+0.244 then gives a kinematic distance of 16.1 kpc.

There are three nebulae in the G46 complex (see Section 6.3) that have very low RRL velocities, $V_{\rm LSR} \lesssim 10$ km s$^{-1}$. Such low velocities give near kinematic distances very close to the Sun, $\lesssim$0.5 kpc. Given their low fluxes and small angular sizes, however, all these sources are likely to be at their far kinematic distances. Finally, G037.468−0.105 is spatially coincident with the W47 H II region complex, and its RRL velocity agrees with other nebulae in the complex. Anderson & Bania (2009) derived a far kinematic distance of 9.6 kpc for these objects so we place G037.468−0.105 there as well.

We give the kinematic distances for the Arecibo HRDS nebulae in Table 5, which lists for each source its name, LSR velocity, tangent-point velocity, near and far distances, KDA resolution, heliocentric distance and its $\pm1\sigma$ uncertainty, Galactocentric radius, and height above the Galactic plane. All kinematic distances and tangent-point velocities are based on the B86 rotation curve. The distance uncertainties are taken from Paper III, which provided percentage uncertainties in kinematic distances for a range of $(\ell, v)$-space loci.

Table 5 shows that of the 19 inner Galaxy nebulae with kinematic distances, 7 (37%) are at the far distance, 12 (63%) are at the tangent-point distance, and none are at the near distance. In comparison, Paper III found that for GBT HRDS sources, 61% are at the far distance, 31% at the tangent-point distance, and 7% at the near distance. Over the longitude range of the Arecibo HRDS, these numbers change to 69%, 30%, and 1%, respectively. Thus, somewhat surprisingly since Arecibo is a more sensitive telescope, a smaller fraction of the Arecibo sample is at the far distance compared to the GBT HRDS. The small number statistics of the Arecibo HRDS distance sample prevent us from drawing any strong conclusions about this.

The dearth of sources at the near distance does, however, imply that the Arecibo HRDS nebulae are on the whole quite distant. The average distance of the Arecibo nebulae is 9.0 kpc, whereas it is 10.1 kpc for the GBT HRDS (9.8 kpc over the Arecibo longitude range) and 8.4 kpc for the Anderson & Bania (2009) H II region sample (8.0 kpc over the Arecibo longitude range). That the GBT HRDS sources are on average more distant is surprising given the weak line intensities of the Arecibo HRDS sample (see Section 6.1). Even if all of the Arecibo HRDS sources without derived kinematic distances were at the far distance, however, the average distance would still be just 9.3 kpc.

## 6. DISCUSSION

### *6.1. Hydrogen Recombination Line Intensities*

The Arecibo HRDS nebulae are some of the faintest H II regions ever observed in RRL emission. The average hydrogen recombination line intensity is 10.1 mK, or 2.5 mJy assuming a gain of 4 K Jy$^{-1}$. These are much weaker recombination lines than those in the GBT HRDS, which has an average line intensity of 35.4 mK, or 17.7 mJy given the GBT gain of 2 K Jy$^{-1}$ (Ghigo et al. 2001). Furthermore, in contrast to the GBT HRDS, the Arecibo HRDS has *only* faint targets. More than 74% of the detected lines have intensities $\lesssim$10 mK, whereas only 18% of GBT HRDS sources meet this criterion. RRL surveys prior to the GBT HRDS observed even brighter targets with higher

**Table 4**
Comparison of Arecibo and GBT HRDS RRL Parameters

| Name | Telescope[a] | $T_L$ (mK) | $\sigma T_L$ (mK) | $\Delta V$ (km s$^{-1}$) | $\sigma \Delta V$ (km s$^{-1}$) | $V_{\rm LSR}$ (km s$^{-1}$) | $\sigma V_{\rm LSR}$ (km s$^{-1}$) | rms (mK) |
|---|---|---|---|---|---|---|---|---|
| G034.133+0.471 | AO | 109.9 | 0.5 | 25.9 | 0.1 | 35.0 | 0.1 | 2.8 |
| | GBT | 117.1 | 0.1 | 25.7 | 0.1 | 34.6 | 0.1 | 2.3 |
| G039.883–0.346 | AO | 98.0 | 0.4 | 33.3 | 0.2 | 58.8 | 0.1 | 1.8 |
| | GBT | 62.2 | 0.1 | 32.2 | 0.1 | 58.9 | 0.1 | 2.7 |
| G052.160+0.706 | AO | 13.3 | 0.5 | 29.0 | 1.4 | 8.2 | 0.5 | 1.8 |
| | GBT | 14.0 | 0.4 | 25.7 | 0.4 | 7.9 | 0.4 | 2.8 |
| G061.720+0.864 | AO | 14.1 | 0.4 | 33.8 | 1.0 | −73.4 | 0.4 | 1.9 |
| | GBT | 18.6 | 0.1 | 27.6 | 0.1 | −75.2 | 0.1 | 1.9 |

**Note.** [a] AO: Arecibo Observatory; GBT: Green Bank Telescope.

**Table 5**
Arecibo HRDS Kinematic Distances

| Name | $V_{\rm LSR}$ (km s$^{-1}$) | $V_{\rm TP}$ (km s$^{-1}$) | $D_{\rm N}$ (kpc) | $D_{\rm F}$ (kpc) | N/F | $D_{\odot}$ (kpc) | $\sigma_D$ (kpc) | $R_{\rm gal}$ (kpc) | $z$ (pc) | Notes[a] |
|---|---|---|---|---|---|---|---|---|---|---|
| G034.591+0.244 | −19.4 | 93.5 | ... | 16.1 | F | 16.1 | 1.1 | 10.3 | 68.5 | Outer |
| G036.996−0.231 | 79.7 | 86.5 | 5.5 | 8.1 | T | 6.8 | ... | 5.3 | −27.4 | TP |
| G037.468−0.105 | 58.7 | 85.2 | 3.9 | 9.6 | F | 9.6 | 0.5 | 5.9 | −17.6 | W47 complex |
| G039.195+0.226 | −21.6 | 80.3 | ... | 15.4 | F | 15.4 | 1.1 | 10.3 | 60.5 | Outer |
| G041.132−0.558 | 65.5 | 74.9 | 4.7 | 8.1 | T | 6.4 | ... | 5.9 | −62.3 | TP |
| G041.881+0.493 | 16.1 | 72.9 | 1.1 | 11.6 | F | 1.1 | 0.1 | 7.7 | 9.1 | HI E/A |
| G043.738+0.114 | 73.1 | 68.0 | 6.1 | 6.1 | T | 6.1 | ... | 5.9 | 12.2 | TP |
| G045.039−0.643 | 61.3 | 64.6 | 4.9 | 7.1 | T | 6.0 | ... | 6.1 | −67.3 | TP |
| G046.176+0.536 | 6.3 | 61.7 | 0.3 | 11.5 | F | 11.5 | 0.7 | 8.3 | 107.2 | G46 complex |
| G046.203+0.535 | 2.1 | 61.6 | ... | 11.8 | F | 11.8 | 0.8 | 8.5 | 109.9 | G46 complex |
| G046.213+0.548 | 5.8 | 61.6 | 0.3 | 11.5 | F | 11.5 | 0.8 | 8.3 | 109.8 | G46 complex |
| G047.094+0.492 | −54.5 | 59.4 | ... | 17.5 | F | 17.5 | 1.4 | 13.2 | 150.2 | Outer |
| G047.100+0.480 | −56.9 | 59.4 | ... | 17.8 | F | 17.8 | 1.5 | 13.6 | 149.4 | Outer |
| G049.738−0.616 | 62.4 | 53.0 | 5.5 | 5.5 | T | 5.5 | ... | 6.5 | −59.1 | TP |
| G050.039−0.274 | 60.9 | 52.3 | 5.5 | 5.5 | T | 5.5 | ... | 6.5 | −26.1 | TP |
| G050.489+0.993 | 57.1 | 51.2 | 5.4 | 5.4 | T | 5.4 | ... | 6.6 | 93.7 | TP |
| G050.785+0.168 | 47.3 | 50.6 | 4.2 | 6.5 | T | 5.4 | ... | 6.7 | 15.7 | TP |
| G051.402−0.890 | 72.8 | 49.1 | 5.3 | 5.3 | T | 5.3 | ... | 6.6 | −82.4 | TP |
| G052.201+0.752 | 8.7 | 47.3 | 0.5 | 9.9 | F | 9.9 | 0.8 | 8.2 | 130.1 | HI E/A; G52 |
| G052.259+0.700 | 7.4 | 47.2 | 0.4 | 10.0 | F | 10.0 | 0.8 | 8.3 | 122.2 | HI E/A; G52 |
| G052.397−0.580 | 67.2 | 46.9 | 5.2 | 5.2 | T | 5.2 | ... | 6.7 | −52.5 | TP |
| G055.159−0.298 | 33.7 | 40.9 | 3.0 | 6.7 | T | 4.9 | ... | 7.2 | −25.2 | TP |
| G063.137+0.252 | 17.1 | 25.9 | 1.6 | 6.1 | T | 3.8 | ... | 7.9 | 16.9 | TP |

**Note.** [a] "TP" = tangent-point distance; "outer" = outer Galaxy.

line intensities (see Paper II, their Figure 9 comparison with Lockman 1989). The relatively low detection rate of Arecibo candidate H II region targets is a direct result of the low mean flux of the Arecibo HRDS nebulae.

### 6.2. Galactic Distribution

The $(\ell, v)$-distribution of Galactic H II regions projected onto that part of the first quadrant Galactic plane accessible to the Arecibo telescope is shown in Figure 4. Seven Arecibo nebulae have velocities beyond the B86 rotation curve tangent-point velocity. They are located in the zone $44° \leqslant \ell \leqslant 60°$, and five of them lie in the range $49\overset{\circ}{.}7 \leqslant \ell \leqslant 52\overset{\circ}{.}4$. The largest discrepancies are for G051.402−0.890, G052.397−0.580, and G059.603+0.911, which are 23.7, 20.3, and 15.1 km s$^{-1}$ beyond the B86 tangent-point velocity, respectively. The location of these five sources in $(\ell, v)$-space is close to the Sagittarius Arm tangent point. Similar, but smaller, velocity deviations beyond the nominal tangent-point velocity can be seen in the H I emission from this part of the Galaxy (see Burton 1966, their feature "C").

The Figure 4 nebulae are the census of *all* currently known H II regions in this zone. Altogether, in the longitude range $\ell \sim 50°–52°$, there are 18 nebulae with velocities that are beyond the terminal velocities predicted by all three of the rotation curve models we use here. Five H II regions have velocities well beyond, $\gtrsim$20–25 km s$^{-1}$, their tangent-point velocities. These excursions are ∼50% higher than the models' average terminal velocity in this direction. This is evidence for strong streaming motions at this location.

We compare in Figure 5 the Galactic radial distribution of the Arecibo HRDS nebulae with that of all previously known H II regions, a sample that includes the GBT HRDS. Over the Arecibo longitude range, we compute the Galactocentric radii for both H II region samples using the B86 rotation curve. The distribution of Arecibo sources shows a strong peak near 6 kpc, similar to what is seen for the previously known sample. The Arecibo nebulae also show a large peak near 8 kpc that is not seen as strongly for the previously known sample. With only 37 sources in the Arecibo HRDS, however, these findings are not particularly robust.

### 6.3. Comments on Individual H II Regions

*G037.498+0.530.* We detect two velocities for this source: 11.6 km s$^{-1}$ and 47.1 km s$^{-1}$. Both lines are of equal intensity. This nebula is near the HRDS source G037.485+0.513, which has three velocities: 4.1 km s$^{-1}$, 50.0 km s$^{-1}$, and 90.8 km s$^{-1}$. These components are all of comparable intensity. Bronfman et al. (1996) detect one CS component with a velocity of 10 km s$^{-1}$ from the nearby position $(\ell, b) = (37\overset{\circ}{.}494, 0\overset{\circ}{.}530)$. This velocity component has also been detected in $NH_3$ by the Red MSX Survey (Urquhart et al. 2011). It therefore seems likely that the RRL source velocity for G037.498+0.530 is 11.6 km s$^{-1}$. One possible scenario is that 90.8 km s$^{-1}$ is the source velocity for GBT HRDS G037.485+0.513 and the ∼50 km s$^{-1}$ component shared by both sources is diffuse. In this scenario, the ∼4–12 km s$^{-1}$ emission is also common to both sources. Finally, the GBT HRDS also detected emission from G037.498+0.530. Further observations are needed to clarify matters.

*G043.738+0.114.* This source has a velocity of 73.1 km s$^{-1}$ and is associated with the GLIMPSE bubble N89. It is near the HRDS source G043.770+0.070, which has a velocity of 70.5 km s$^{-1}$ and is also associated with a GLIMPSE bubble, N90 (see Figure 1). Neither object has a distance determination as yet.

*G046.017+0.264.* Because of its MIR morphology and broad line width, this source might be a PN. Urquhart et al. (2009) classify this source as a PN. Anderson et al. (2012b) show that

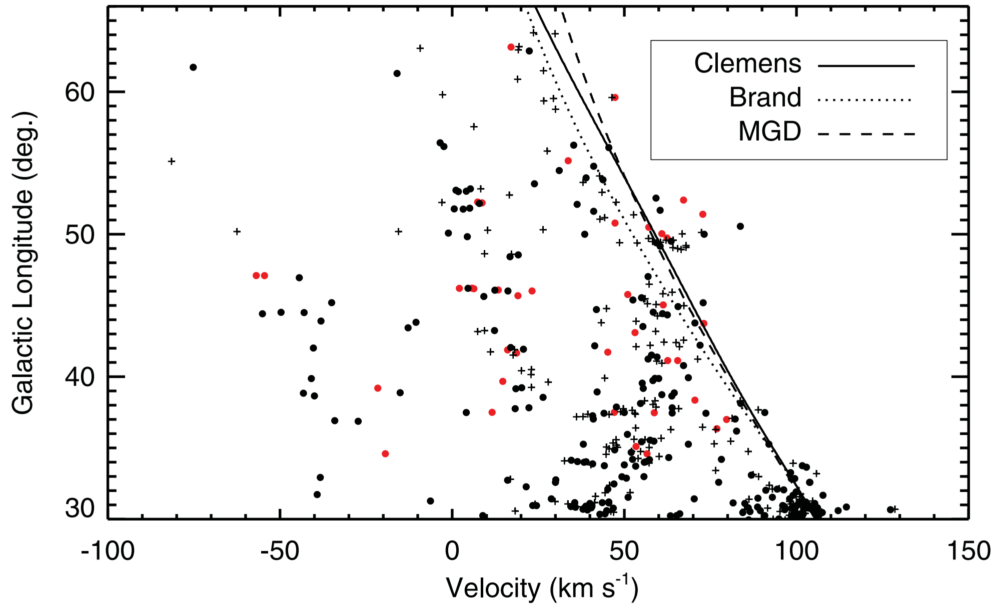


**Figure 4.** H ii region longitude–velocity diagram for the first quadrant Galactic plane visible to the Arecibo telescope. Shown is the current census of all known H ii regions in this zone from: the Arecibo HRDS (red circles), the GBT HRDS (black circles), and nebulae known prior to the GBT HRDS (black crosses; see Paper II). Tangent-point velocity loci for the Clemens (1985), Brand (1986), and McClure-Griffiths & Dickey (2007) rotation curves are drawn as solid, dotted, and dashed lines, respectively. In the longitude range $\ell \sim 50°–52°$, there are 18 nebulae with velocities that are beyond the terminal velocities predicted by all three of the rotation curve models.

(A color version of this figure is available in the online journal.)

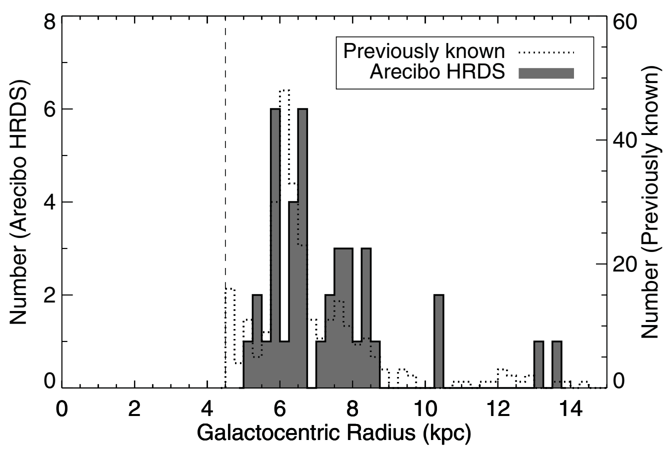


**Figure 5.** Galactic radial distribution of H ii regions. Arecibo HRDS nebulae are the gray filled histogram and the previously known sample of H ii regions, including the GBT HRDS, is the dotted line histogram. Only nebulae located in the longitude range of the Arecibo HRDS are included here. The vertical dashed line shows the minimum Galactocentric radius sampled by the present study.

IR colors can be used to distinguish between H ii regions and PNe. MIR aperture photometry for this source using GLIMPSE, MIPSGAL, and *WISE* (Wright et al. 2010) data, however, is inconclusive. FIR data would help resolve the nature of this object.

*G046.176+0.536, G046.203+0.535, & G046.213+0.548.* These three sources are in a complex we call here G46 and have velocities ranging from 2.1 km $s^{-1}$ to 6.3 km $s^{-1}$. G046.203+0.535 is a GBT HRDS nebula, but the GBT beam included emission from the other two sources. Paper III did not establish a distance because the radio continuum emission is too faint. The small angular size, weak continuum flux, and low LSR velocities of the nebulae in this complex favor the far distance. We thus place all three sources at the far kinematic distance of 11.5 kpc.

*G052.201+0.752 & G052.259+0.700.* These two sources and the nearby re-observed GBT HRDS source G052.160+0.706 all have emission in the off-source direction. The source velocities for G052.201+0.752, G052.259+0.700, and G052.160+0.706 are 8.7 km $s^{-1}$, 7.4 km $s^{-1}$, and 8.2 km $s^{-1}$, respectively. The off-source velocities are 53.7 km $s^{-1}$, 51.6 km $s^{-1}$, and 52.0 km $s^{-1}$. We fit the negative-intensity off-source emission simultaneously with that of the on-source emission. The fits to the on-source emission are the line parameters given in Table 2. The lines are well-separated in velocity (see Figure 3) so the line parameters do not appear to be strongly affected by the off-source emission. The derived LSR velocities do not change when the lines are fit individually. Furthermore, for G052.160+0.706, the Arecibo and GBT HRDS velocities match.

The off-source positions, $(\ell, b) = (52^\circ\!.884, -0^\circ\!.505)$, $(52^\circ\!.942, -0^\circ\!.557)$, and $(52^\circ\!.844, -0^\circ\!.548)$, all coincide with a single large, diffuse H ii region. There is a separate compact H ii region along the eastern border of the diffuse region, G052.940−0.588. Lockman (1989) found RRL emission for this nebula at a velocity of 43.5 km $s^{-1}$. The velocity discrepancy between this compact H ii region and the ∼53 km $s^{-1}$ off-source emission is puzzling since both sources are spatially coincident. Perhaps the two nebulae are not physically associated at all.

### 6.4. *The G52 Complex*

The three H ii regions just discussed are part of an even larger complex that is comprised of at least seven compact nebulae. We call this complex "G52" and show this complicated field in Figure 6. The green numbers and vectors in the upper left panel mark the RRL velocities (in km $s^{-1}$) of the two Arecibo HRDS nebulae, G052.201+0.752 and G052.259+0.700, whereas GBT HRDS nebulae are marked in cyan. Watson et al. (2003) measure a −3.0 km $s^{-1}$ RRL velocity for the yellow-marked nebula,

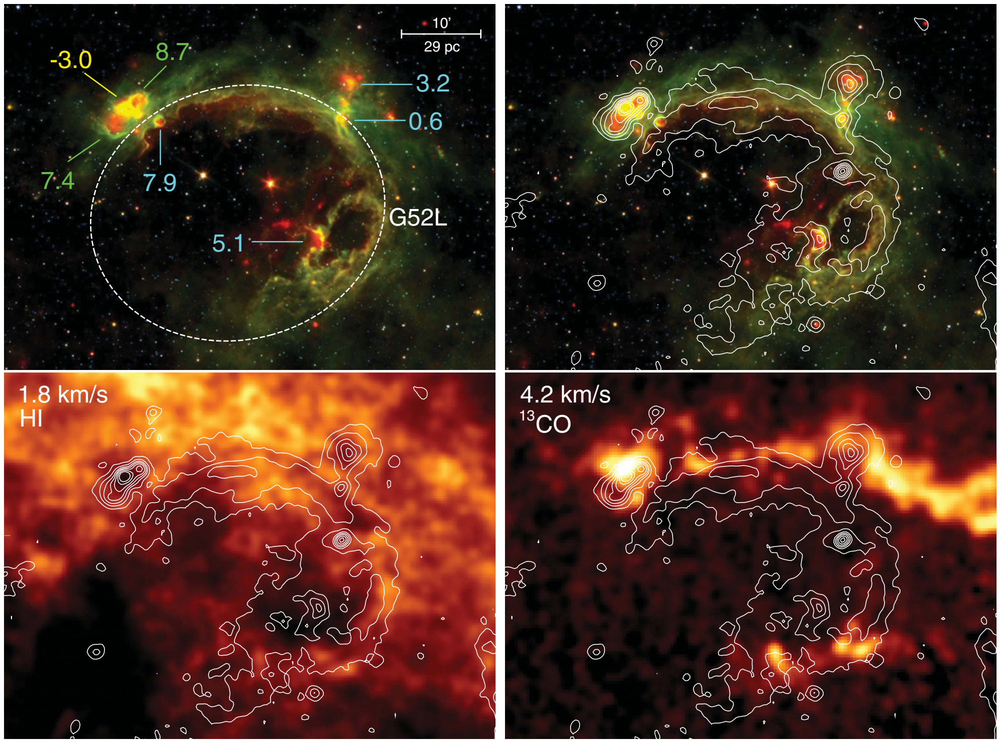


**Figure 6.** Multi-wavelength images of the G52 complex. Each is centered at $(\ell, b) = (51\overset{\circ}{.}97, 0\overset{\circ}{.}57)$ and shows a region spanning $1^\circ \times 0\overset{\circ}{.}75$ in Galactic coordinates. The scale bar in the top left panel shows 10′, which is 29 pc at a distance of 10 kpc; the entire field shown is 175 × 130 pc. G52L is the large half-circle structure open to the southeast, marked with a white dashed ellipse in the top left panel. Contours are of VGPS 21 cm continuum emission at levels of 9, 12, 16, 20, 25, 32, and 40 K. Background images for the top two panels are *Spitzer* data: MIPSGAL 24 $\mu$m (red), GLIMPSE 8.0 $\mu$m (green), and GLIMPSE 3.6 $\mu$m (blue). In the top left panel, the RRL velocities (in $\text{km s}^{-1}$) and vectors point to different nebulae in this complex. Colors identify the source of these data: green for this work, cyan for the GBT HRDS, and yellow for Watson et al. (2003). The bottom left panel shows a single H I channel from the VGPS at a velocity of 1.8 $\text{km s}^{-1}$. The bottom right panel shows a single $^{13}$CO channel from the GRS at a velocity of 4.2 $\text{km s}^{-1}$. Both bottom panel images are spatially smoothed with a 1′ FWHM Gaussian kernel.

(A color version of this figure is available in the online journal.)

G052.230+0.740, using Arecibo with a 1′ beam. Lockman (1989) finds a 2.8 $\text{km s}^{-1}$ velocity for this same source with the 3′ NRAO 140 Foot telescope beam.

We adopt here a kinematic distance of 10 kpc for the G52 complex. This is based on our H I E/A measurements for the two Arecibo nebulae, G052.201+0.752 and G052.259+0.700, that support the ∼10 kpc far distance. Furthermore, GBT HRDS G052.160+0.706 is nearby and has a velocity of 7.9 $\text{km s}^{-1}$ (Paper II). Paper III found a far kinematic distance of 10 kpc for this nebula. Finally, using the Lockman (1989) velocity for G052.230+0.740, Anderson & Bania (2009) found strong evidence for the far kinematic distance (which is further supported by the negative velocity measured by Watson et al. 2003).

The spatial distribution of the compact nebulae in the G52 field defines the border of an even larger structure that we call "G52L," which is outlined by the dashed ellipse in the upper left panel of Figure 6. While there are many observations of the smaller compact H II regions in the field, due to its faint radio flux, G52L has not yet been observed in RRL emission. Based on its MIR and radio continuum morphology together with the ongoing star formation on its borders, G52L is almost certainly a large H II region.

G52L seems to be an evolved H II region that has displaced a significant amount of material through its expansion, leaving a low density, low emission measure internal cavity. An H I shell spatially coincident with the photodissociation region (PDR) seen at 8.0 $\mu$m is clearly visible (see Figure 6, bottom left panel). The velocity of this shell, 1.8 $\text{km s}^{-1}$, suggests that G52L is associated with the smaller compact H II regions. To our knowledge, this shell has not been identified previously as an H II region. In the bottom right panel of Figure 6, we show $^{13}$CO emission at 4.2 $\text{km s}^{-1}$ from the Galactic Ring Survey (GRS; Jackson et al. 2006). There is $^{13}$CO gas along the north and south PDRs of G52L. This gas may be tracing future sites of star formation in the region. These H I and $^{13}$CO shells indicate that a significant amount of material has been displaced by the expansion of G52L.

G52L may be the largest single H II region in the Galaxy. The PDR region traced at 8.0 $\mu$m in Figure 6 is ∼30′ in diameter. Using the distance to the compact sources, ∼10 kpc, this corresponds to a physical diameter of 90 pc (the H I and $^{13}$CO shells give the same result). This is about 40% the MIR size we measure for the Large Magellanic Cloud's 30 Doradus nebula, which is the largest H II region in the local universe (Freedman & Madore 2010).

We estimate the size of various other large, well-known H II regions using GLIMPSE 8.0 $\mu$m and *WISE* 12 $\mu$m data.[6] We find that G52L is three times larger than W43 (15′ diameter and 5.7 kpc distance from Anderson & Bania 2009), over twice as large as the G305 complex (30′ diameter and 4 kpc distance from Russeil et al. 1998; see recent paper by Hindson et al. 2012), about twice the size of W5-E (50′ diameter and assuming the 2.0 kpc distance for W3 from Xu et al. 2006 also applies to W5; see recent paper L. Deharveng et al. 2012, submitted),

[6] Both data sets trace H II region PDRs so that they are equivalent for our purposes (Anderson et al. 2012b).

about twice the size of W5-W (1° diameter and the same 2.0 kpc distance), about twice as large as CTB 102 (35′ diameter, not including any associated radio continuum "filaments," and 4.3 kpc distance from Arvidsson et al. 2009) and three times larger than W51 (20′ diameter of main H II region W51B from Westerhout 1958 and 5.6 kpc distance from Anderson & Bania 2009).

A region as large and energetic as G52L can shape the evolution of subsequent generations of star formation in its vicinity. Paper II and Deharveng et al. (2010) show that nearly all cataloged IR bubbles enclose H II regions. G52L is spatially coincident with the infrared dust bubble N109 in the Churchwell et al. (2006) compilation, while the smaller loop to the southwest has been separately cataloged as N108. There is no evidence, however, that N109 and N108 are not part of the same large source. Interestingly, most of the small H II regions are also spatially coincident with infrared dust bubbles: G052.160+0.706 with N110, G052.201+0.752 with N111, G052.230+0.740 with N113, and G052.259+0.700 with N114.[7] This high density of bubble H II regions is unusual and may indicate that the G52 local environment is conducive to their formation.

We hypothesize that there may be many other large, evolved Galactic H II regions similar to G52L that, due to their low flux densities, remain undiscovered. G52L is 10 kpc distant and has a 1.4 GHz flux density of ~11 Jy. This implies an ionizing luminosity of $\sim 10^{49.9}\,\mathrm{s}^{-1}$, equivalent to two main-sequence O4 stars or ~11 main-sequence 07 stars (Sternberg et al. 2003). Because it is relatively faint, G52L is not in the Murray & Rahman (2010) catalog of large massive star-forming regions. Its exclusion hints that other, yet to be discovered, luminous diffuse H II regions such as G52L may make a significant contribution to the total ionization of the Galaxy.

## 7. SUMMARY

Using the Arecibo Observatory at X band (3 cm), we detect RRL emission from 37 previously unknown H II regions in the Galactic zone $66° \geqslant \ell \geqslant 31°$ and $|b| \leqslant 1°$. As in the GBT HRDS, the Arecibo HRDS candidate H II region targets are selected based on spatially coincident 24 $\mu$m and 20 cm emission that has a similar morphology and angular extent. Compared to the GBT HRDS, the Arecibo HRDS targets are fainter, smaller in angular size, or are in more crowded fields. The Arecibo HRDS nebulae are among the faintest ever detected in RRL emission. Only 58% of the Arecibo HRDS candidate H II regions show RRL emission, whereas the detection rate for GBT HRDS targets was 95%. We do not really know why the discovery rate for Arecibo H II region candidates is so low compared with that for the GBT HRDS. It may just be the case that the relatively low detection rate of Arecibo H II region candidates is a direct result of the low mean flux of the Arecibo HRDS nebulae. Despite having an average spectral sensitivity a factor of two better, the mean signal-to-noise ratio (S/N) for Arecibo H II region detections is 5.0 compared to the 17.7 S/N for GBT HRDS nebulae. Perhaps the GBT census had already detected the bulk of the H II regions in this part of the Milky Way that are detectable by Arecibo with reasonable integration times. We also may be finding the first indication of a real drop off in the H II region luminosity distribution.

The Arecibo HRDS enhances the census of regions of massive star formation for that part of the first quadrant Galactic disk that is accessible to the Arecibo telescope. This census reveals five H II regions near $\ell \sim 50°$ that have velocities $\gtrsim$20–25 km s$^{-1}$ beyond the tangent-point velocity in this direction. This is evidence for strong streaming motions at this location. Over the Arecibo longitude range, the Galactic radial distribution of H II regions shows peaks at ~6 kpc and ~8 kpc. The 8 kpc peak for the Arecibo HRDS is more prominent than that for the distribution of H II regions known previously.

We derive kinematic distances for 23 Arecibo HRDS nebulae. Four of these have negative LSR velocities, placing them unambiguously in the outer Galaxy. Of the remaining sources, 12 are at the tangent-point distance and the others are at the far kinematic distance.

We find, apparently for the first time, a large H II region, G52L, that is a member of a complex of H II regions 10 kpc distant. G52L may be the largest single H II region in the Galaxy. It is physically larger than all the well-known H II regions we discuss here and is about 40% the size of 30 Doradus in the Large Magellanic Cloud. G52L is associated with a 30′ diameter H I shell that is spatially coincident with its PDR, and also with $^{13}$CO emission on its northern and southern boundaries. Together with most of the H II regions in the complex, G52L has a bubble morphology when observed at mid-infrared wavelengths. This concentration of bubbles is unusual and may indicate something about the local environment.

The Arecibo Observatory is operated by SRI International under a cooperative agreement with the National Science Foundation (AST-1100968), and in alliance with Ana G. Méndez-Universidad Metropolitana, and the Universities Space Research Association. This research has made use of NASA's Astrophysics Data System Bibliographic Services and the SIMBAD database operated at CDS, Strasbourg, France. The National Radio Astronomy Observatory is a facility of the National Science Foundation operated under cooperative agreement by Associated Universities, Inc. T.M.B.'s research was partially supported by NSF award AST 0707853.

*Facility*: Arecibo

## APPENDIX

## THE HRDS WEB SITE

All the Arecibo HRDS data are now incorporated in our HRDS Web site, http://go.nrao.edu/hrds, where one can view the three-color images (Figure 1) and the ⟨H n α⟩ recombination line spectra (Figure 3). One can also download the contents of Tables 1, 2, and 5. As we continue to extend the HRDS, all future data will also be available on this site.

## REFERENCES

Anderson, L. D., & Bania, T. M. 2009, ApJ, 690, 706
Anderson, L. D., Bania, T. M., Balser, D. S., & Rood, R. T. 2011, ApJS, 194, 32
Anderson, L. D., Bania, T. M., Balser, D. S., & Rood, R. T. 2012a, ApJ, 754, 62
Anderson, L. D., Zavagno, A., Barlow, M. J., García-Lario, P., & Noriega-Crespo, A. 2012b, A&A, 537, A1
Araya, E., Hofner, P., Churchwell, E., & Kurtz, S. 2002, ApJS, 138, 63
Arvidsson, K., Kerton, C. R., & Foster, T. 2009, ApJ, 700, 1000
Balser, D. S. 2006, AJ, 132, 2326
Bania, T. M., Anderson, L. D., Balser, D. S., & Rood, R. T. 2010, ApJ, 718, L106
Benjamin, R. A., Churchwell, E., Babler, B. L., et al. 2003, PASP, 115, 953

[7] Notably missing from this list is N112, which is yet to be observed in RRL emission. Nonetheless, based on its MIR and radio morphology, N112 is probably an H II region.

Brand, J. 1986, PhD thesis, Leiden Univ., Netherlands
Broadbent, A., Osborne, J. L., & Haslam, C. G. T. 1989, MNRAS, 237, 381
Bronfman, L., Nyman, L.-A., & May, J. 1996, A&AS, 115, 81
Burton, W. B. 1966, Bull. Astron. Inst. Neth., 18, 247
Carey, S. J., Noriega-Crespo, A., Mizuno, D. R., et al. 2009, PASP, 121, 76
Caswell, J. L., & Haynes, R. F. 1987, A&A, 171, 261
Churchwell, E., Povich, M. S., Allen, D., et al. 2006, ApJ, 649, 759
Clemens, D. P. 1985, ApJ, 295, 422
Deharveng, L., Schuller, F., Anderson, L. D., et al. 2010, A&A, 523, A6
Deharveng, L., Zavagno, A., Anderson, L. D., et al. 2012, arXiv:1209.2907
Freedman, W. L., & Madore, B. F. 2010, ARA&A, 48, 673
Ghigo, F., Maddalena, R., Balser, D., & Langston, G. 2001, GBT Commissioning Memo 10
Haslam, C. G. T., & Osborne, J. L. 1987, Nature, 327, 211
Helfand, D. J., Becker, R. H., White, R. L., Fallon, A., & Tuttle, S. 2006, AJ, 131, 2525
Hindson, L., Thompson, M. A., Urquhart, J. S., et al. 2012, MNRAS, 421, 3418
Jackson, J. M., Rathborne, J. M., Shah, R. Y., et al. 2006, ApJS, 163, 145
Kolpak, M. A., Jackson, J. M., Bania, T. M., Clemens, D. P., & Dickey, J. M. 2003, ApJ, 582, 756
Kuchar, T. A., & Bania, T. M. 1994, ApJ, 436, 117
Levine, E. S., Heiles, C., & Blitz, L. 2008, ApJ, 679, 1288
Lockman, F. J. 1989, ApJS, 71, 469
McClure-Griffiths, N. M., & Dickey, J. M. 2007, ApJ, 671, 427
Murray, N., & Rahman, M. 2010, ApJ, 709, 424
Pestalozzi, M. R., Minier, V., & Booth, R. S. 2005, A&A, 432, 737
Reifenstein, E. C., Wilson, T. L., Burke, B. F., Mezger, P. G., & Altenhoff, W. J. 1970, A&A, 4, 357
Russeil, D., Georgelin, Y. M., Amram, P., et al. 1998, A&AS, 130, 119
Sewilo, M., Churchwell, E., Kurtz, S., Goss, W. M., & Hofner, P. 2004, ApJ, 605, 285
Sternberg, A., Hoffmann, T. L., & Pauldrach, A. W. A. 2003, ApJ, 599, 1333
Stil, J. M., Taylor, A. R., Dickey, J. M., et al. 2006, AJ, 132, 1158
Urquhart, J. S., Hoare, M. G., Purcell, C. R., et al. 2009, A&A, 501, 539
Urquhart, J. S., Morgan, L. K., Figura, C. C., et al. 2011, MNRAS, 418, 1689
Watson, C., Araya, E., Sewilo, M., et al. 2003, ApJ, 587, 714
Wenger, T. V., Bania, T. M., Balser, D. S., & Anderson, L. D. 2012, ApJ, submitted
Westerhout, G. 1958, Bull. Astron. Inst. Neth., 14, 215
Wilson, T. L., Mezger, P. G., Gardner, F. F., & Milne, D. K. 1970, A&A, 6, 364
Wood, D. O. S., & Churchwell, E. 1989, ApJS, 69, 831
Wright, E. L., Eisenhardt, P. R. M., Mainzer, A. K., et al. 2010, AJ, 140, 1868
Xu, Y., Reid, M. J., Zheng, X. W., & Menten, K. M. 2006, Science, 311, 54